Journal of Solid State Chemistry **159,** 215–222 (2001)
doi:10.1006/jssc.2001.9187, available online at http://www.idealibrary.com on IDEAL®

Electronic and Magnetic Properties Due to Co Ions in $La_{0.9}Sr_{0.1}Fe_{1-x}Co_xO_3$

H. Nakatsugawa[1] and E. Iguchi

Materials Science, Department of Mechanical Engineering and Materials Science, Faculty of Engineering, Yokohama National University, Tokiwadai, Hodogaya-Ku, Yokohama 240-8501 Japan

Received December 21, 2000; in revised form March 22, 2001; accepted March 26, 2001

Variations in physical properties due to Co ions in $La_{0.9}Sr_{0.1}Fe_{1-x}Co_xO_3$ ($x \leq 0.5$) in which short-range ferromagnetic orders are expected to work predominantly at a rather large x have been investigated so as to elucidate Co states. dc and ac measurements indicate that a hopping process of small polarons dominates electronic conduction, but there is a large reduction in hopping energy when x increases from 0.1 to 0.5. This reduction is related to the structural transition induced by an increase in Co content. A spin-glass phase due to short-range ferromagnetic orders is recognized for $x = 0.5$ in magnetic measurements. A Curie–Weiss relation realized for $x = 0.5$ and comparison of the thermopower extrapolated experimentally at $T \to \infty$ with magnitudes estimated theoretically deduce that all or most of Co ions in $La_{0.9}Sr_{0.1}Fe_{1-x}Co_xO_3$ are HS Co^{3+} and IS Co^{4+} ions.

Key Words: **short range ferromagnetic order; spin-glass phase; double-exchange interaction, Curie–Weiss relation; effective magnetic moment; spin-state; Fe-antiferromagnetism; small polaron; hopping energy; thermopower.**

1. INTRODUCTION

The present study investigates electronic and magnetic properties due to Co ions in $La_{0.9}Sr_{0.1}Fe_{1-x}Co_xO_3$. Since $La_{0.9}Sr_{0.1}Fe_{1-x}Co_xO_3$ is a solid solution of $La_{0.9}Sr_{0.1}FeO_3$ and $La_{0.9}Sr_{0.1}CoO_3$, it is useful to understand outlines of the experiments carried out previously on end members, $La_{1-x}Sr_xFeO_3$ and $La_{1-x}Sr_xCoO_3$, for a start. $LaFeO_3$, the end member of $La_{1-x}Sr_xFeO_3$, is an antiferromagnetic insulator with Néel temperature, $T_N \cong 750$ K. With increasing x up to 0.4, Néel temperature lowers and resistivity reduces (1). $La_{1-x}Sr_xFeO_3$ crystallizes in orthorhombic structure (*Pbnm*) and the valence of Fe ions in this system varies from $+3$ ($3d^5$, $x = 0$) to $+4$ ($3d^4$, $x = 1$) with increasing x. XAS (soft X-ray absorption spectroscopy) spectrum indicates that the main component in $LaFeO_3$ ground state is high-spin (HS) state ($3d^5$, $t_{2g}^3 e_g^2$) (2). Since the holes created by Sr^{2+} substitution for La^{3+} go to states of primary O $2p$ character, the main component of the ground state transfers to $3d^5\underline{L}$ in $La_{1-x}Sr_xFeO_3$, where $\underline{L}$ denotes a ligand hole. Thus, Sr substitution brings about the strong covalent character in the ground state. This is also evidenced by XPS (X-ray photoelectron spectra) experiment (3).

It is well known that $LaCoO_3$ exhibits the transport and magnetic properties peculiar to this oxide and that thermally induced spin-state transition of Co^{3+} ions causes these properties (4). At very low temperature, Co^{3+} ions are all in low-spin (LS) state (t_{2g}^6) because crystal-field splitting strength (10 Dq) is slightly larger than Hund's rule coupling energy (J). Such a small energy difference between 10 Dq and J allows thermal excitation of HS state ($t_{2g}^4 e_g^2$) or intermediate-spin (IS) state ($t_{2g}^5 e_g^1$) with increasing temperature (5). $La_{1-x}Sr_xCoO_3$ system has been extensively studied (6–13). Sr-substitution for La oxidizes Co^{3+} ($3d^6$) partially into Co^{4+} ($3d^5$), and several spin configurations have been proposed for Co^{4+} in $La_{1-x}Sr_xCoO_3$, i.e., LS (t_{2g}^5) (14), HS ($t_{2g}^3 e_g^2$) (6), or IS ($t_{2g}^4 e_g^1$) states (15). When x in $La_{1-x}Sr_xCoO_3$ is small ($0.03 \leq x \leq 0.07$), strongly hybridized $3d$–$2p$ bands due to e_g electrons on IS Co^{3+} ($t_{2g}^5 e_g^1$) are formed and the holes with a strong component of $d_{x^2-y^2}$ parentage of the e_g state ($3d^6\underline{L}$-ligand holes) move within the lattice by hopping (16). Since this hybridization becomes strong with increasing x, the similar conduction is expected in $La_{0.9}Sr_{0.1}CoO_3$. $La_{1-x}Sr_xCoO_3$ crystallizes in rhombohedral structure ($R\bar{3}C$) and a paramagnetic to ferromagnetic phase transition occurs at $x \cong 0.2$ (17, 18). $La_{1-x}Sr_xCoO_3$ includes a spin-glass phase ($x \leq 0.18$) and a cluster-glass phase ($0.18 < x \leq 0.25$) at $T \leq T_g$ and a long-range ferromagnetic ordered phase ($0.25 < x \leq 0.5$) below T_C, where T_g and T_C are spin-glass freezing temperature and Curie–Weiss temperature, respectively (19).

Magnetic and structural properties in the $La_{0.7}Sr_{0.3}Fe_{1-x}Co_xO_3$ system were explored by neutron diffraction and ac magnetization measurements (20). A transition from

[1] To whom correspondence should be addressed. Fax: +81-45-331-6593. E-mail: hiro@post.me.ynu.ac.jp.

0022-4596/01 $35.00

orthorhombic to rhombohedral structure occurs at $x = 0.5$. This oxide system exhibits ferromagnetic behavior at $x \geq 0.6$, but antiferromagnetic feature at $x \leq 0.2$. In the intermediate range of $0.3 \leq x \leq 0.5$, the competition between ferromagnetic structure mainly due to Co and antiferromagnetic structure based upon Fe causes the complex behavior. The most significant Co effect in $La_{0.7}Sr_{0.3}Fe_{1-x}Co_xO_3$ is to enhance Co^{3+}–O^{2-}–Co^{4+} double-exchange (DE) interaction (21–23), which results in long-range ferromagnetic orders. Spin states of Co ions are, however, still unknown. The replacement of Fe with Co decreases unit cell volume and this is due to the ionic radius of Co smaller than Fe.

Referring to the experiment on $La_{1-x}Sr_xCoO_3$ described above, short-range ferromagnetic orders must be mainly responsible for magnetic nature, resulting in a spin-glass phase, when the amount of holes is small because x in $La_{1-x}Sr_xCoO_3$ also represents density of holes, but long-range ferromagnetism is expected when the amount of holes is large. $La_{0.7}Sr_{0.3}Fe_{1-x}Co_xO_3$ ($x \geq 0.5$) does not contain a spin-glass phase because of long-range ferromagnetic orders due to the large amount of holes. In $La_{0.9}Sr_{0.1}Fe_{1-x}Co_xO_3$, short-range ferromagnetic orders are expected to dominate magnetic properties at a rather large x, consequently resulting in a spin-glass phase, although this material must involve mainly antiferromagnetic natures based upon Fe-antiferromagnetism when x is small as well as $La_{0.7}Sr_{0.3}Fe_{1-x}Co_xO_3$. Since $La_{0.7}Sr_{0.3}Fe_{1-x}Co_xO_3$ has been investigated in detail (20), it is very interesting to elucidate Co-states in a material in which short-range ferromagnetic orders work predominantly.

From this point of view, the present study has investigated Co-effects on variations of physical properties in $La_{0.9}Sr_{0.1}Fe_{1-x}Co_xO_3$. This experiment could provide essential knowledge of Co-states in this system. Furthermore, the low density of holes in $La_{0.9}Sr_{0.1}Fe_{1-x}Co_xO_3$ compared with $La_{0.7}Sr_{0.3}Fe_{1-x}Co_xO_3$ results in rather high resistivity. As our previous reports indicate (16, 24–33), dc conductivity measurements on rather less conductive insulators are supported by ac measurements and can provide very reliable information on electronic conduction. The combination of dc and ac measurements is impossible for $La_{0.7}Sr_{0.3}Fe_{1-x}Co_xO_3$ because of high conductivity due to the high density of holes, but possible partially for $La_{0.9}Sr_{0.1}Fe_{1-x}Co_xO_3$. Thermopower measurement is also employed because the recent theoretical study on the $T \to \infty$ limit of the thermopower (34, 35) makes it possible to elucidate spin states of Co ions by comparing the theoretical value with the experimental one. Magnetic measurement is indispensable in elucidation of magnetic properties and spin-states of ions. Based upon a strategy like this, measurements of dc conductivity, ac properties, thermopower and magnetic properties have been carried out on $La_{0.9}Sr_{0.1}Fe_{1-x}Co_xO_3$ so as to investigate variations in electronic and magnetic properties due to a change in Co content, and then the results have been discussed in terms of electronic states of Co ions.

2. EXPERIMENTAL DETAILS

Polycrystalline specimens of $La_{0.9}Sr_{0.1}Fe_{1-x}Co_xO_3$ ($x = 0.1$ and 0.5) were prepared by the conventional ceramic method, using dried La_2O_3, $SrCO_3$, Co_3O_4, and Fe_2O_3 powders (4N grades) as starting materials. The appropriate mixtures of these powders were calcined in air at 1373 K for 1 day. Then, the powders were pressed into pellets and finally sintered in air at 1623 K for 1 day. All of the sintered pellets were analyzed, using an X-ray diffractometer with a graphite monochromator and Cu$K\alpha$ radiation with step scanning. Silicon powder (5N grade) was used as an internal standard for precise lattice parameter measurements. The powder X-ray diffraction patterns showed formation of a single-phase compound and no impurity line was involved. Chemical analyses by redox titration determined the oxygen contents of the specimens, i.e., $La_{0.9}Sr_{0.1}Fe_{0.9}Co_{0.1}O_{2.99}$ and $La_{0.9}Sr_{0.1}Fe_{0.5}Co_{0.5}O_{2.98}$, as slightly oxygen-deficient in both specimen. The experimental error of the oxygen content is within $\pm 3\%$.

Using an HP 4284A LCR meter with the frequency range 20 Hz to 1 MHz, the capacitance and conductance were obtained as functions of temperature by the four-terminal pair ac impedance measurement method. The measured values of the capacitance and the conductance were corrected by calibrating the capacitance and the resistance of the leads as zero. An In–Ga alloy in a 7 : 3 ratio was used for the electrode. Evaporated gold was also used for the electrode, but no significant difference was found in the experimental results. In order to check the surface capacitance effect, capacitance measurements were carried out at 200 K in the frequency range of 10 kHz to 1 MHz by changing the thickness of the specimen from 1.2 to 0.6 mm, and the dielectric constants were independent of the thickness. Thus, surface effects were not included in the dielectric properties obtained in the present experiment.

Thermopower was measured with a precision digital multimeter in the temperature range of 100–330 K in a home-made device. Both ends of the specimen were placed between two blocks machined from oxygen-free high conductivity copper; a temperature difference of 5–10 K was set up between the two electrodes. Copper-constantan thermocouples were welded to the reverse side of each copper plate to measure both the temperature and the thermoelectric voltage. A Keithley 619 resistance bridge, an Advantest TR 6871 digital multimeter, and an Advantest R 6161 power supply were used for dc conductivity measurements by the four-probe method. Copper-constantan thermocouple precalibrated at 4.2, 77, and 273 K was used for the temperature measurements. The magnetic susceptibilities were

measured by using SQUID (Quantum Design, MPMS). Susceptibility–temperature (χ–T) curves were measured under zero-field cooled (ZFC) and field cooled (FC) conditions at an applied field.

3. RESULTS AND DISCUSSION

3.1. Lattice Structure

Figures 1a and 1b show the powder X-ray diffraction (XRD) patterns of $La_{0.9}Sr_{0.1}Fe_{0.9}Co_{0.1}O_3$ ($x = 0.1$) and $La_{0.9}Sr_{0.1}Fe_{0.5}Co_{0.5}O_3$ ($x = 0.5$). The specimen with $x = 0.1$ exhibits an XRD pattern of orthorhombic structure including four chemical formulae per unit cell (*Pbnm*) (20), and Miller indices attached on Fig. 1a are based upon this structure. It is also possible to index the XRD pattern in Fig. 1b if rhombohedral structure with two chemical formula units per cell ($R\bar{3}C$) is accepted (20). $La_{0.9}Sr_{0.1}Fe_{1-x}Co_xO_3$ involves then a phase transition from orthorhombic structure with a *Pbnm* space group to rhombohedral with $R\bar{3}C$ with increasing x. The least-mean-squares fitting methods yield $a = 5.542$ Å, $b = 5.534$ Å, and $c = 7.811$ Å for $x = 0.1$, and $a_H = 5.491$ Å and $c_H = 13.254$ Å for $x = 0.5$.

3.2. Conductivity

Following the theoretical procedures of a complex-plane impedance analysis (36–38), Fig. 2 demonstrates impedance plots at 100, 150, and 250 K for the specimen with $x = 0.1$. The impedance analysis was, however, impossible for $x = 0.5$ because of high conductivity. As described in details elsewhere (16, 27–33), the impedance analysis distinguishes bulk conduction from others. Figure 3 illustrates Arrhenius relations of σT and $1/T$, employing bulk conductivity and four-probe dc conductivity for $x = 0.1$ and dc conductivity for $x = 0.5$. Since the impedance analysis also distinguishes the total resistance in bulks and boundaries from others (16, 27–33), Fig. 3 includes the plots of conductivity corresponding to the total resistance of bulks and boundaries for $x = 0.1$, which agree well with the plots of four-probe dc conductivity as expected (36–38). The linear relation between σT and $1/T$ in each specimen is in favor of adiabatic hopping conduction in $La_{0.9}Sr_{0.1}Fe_{1-x}Co_xO_3$ because the polaron theory predicts the following formula for adiabatic polaronic conduction:

$$\sigma T \propto \exp\left(-\frac{W_H}{k_B T}\right), \qquad [1]$$

where W_H is hopping energy of small polarons and k_B is Boltzmann's constant (39, 40). As for $x = 0.1$, hopping energy obtained in dc conductivity is nearly equal to the

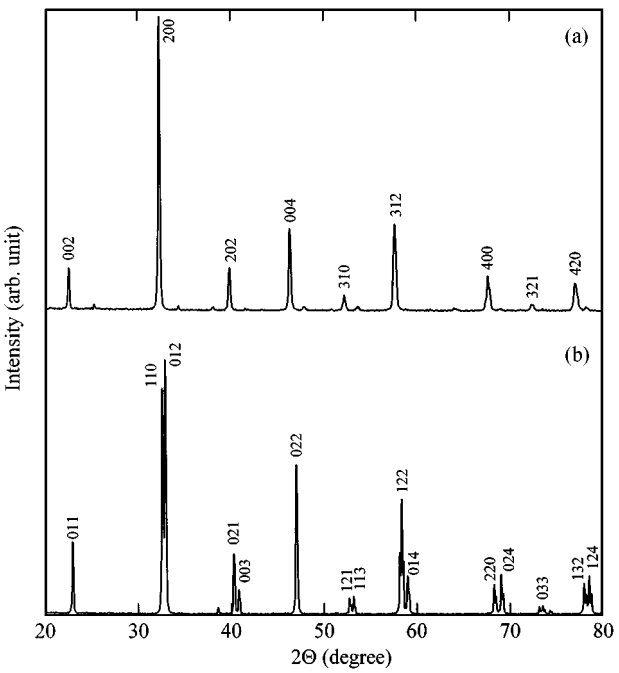

FIG. 1. X-ray diffraction patterns of the $La_{0.9}Sr_{0.1}Fe_{1-x}Co_xO_3$ system: (a) $x = 0.1$ and (b) $x = 0.5$.

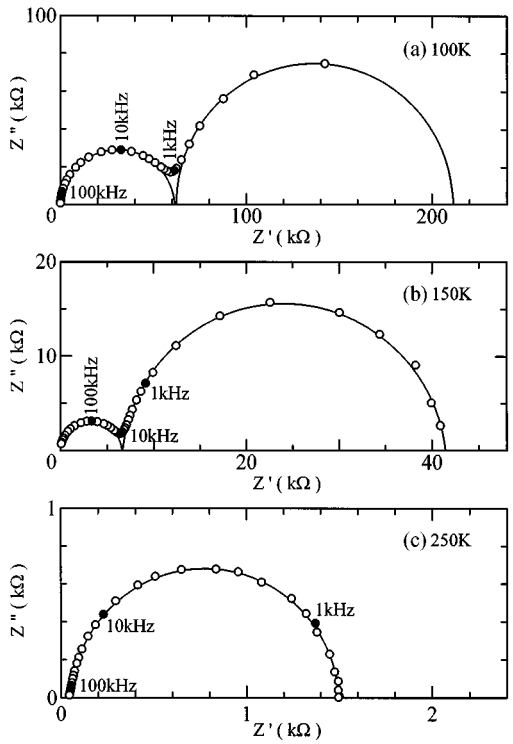

FIG. 2. Complex-plane impedance analyses for $La_{0.9}Sr_{0.1}Fe_{1-x}Co_xO_3$ specimen with $x = 0.1$ at several temperatures; (a) 100 K, (b) 150 K and (c) 250 K, where Z' and Z'' represent real and imaginary parts of the total impedance at each applied frequency. The highest resistance value of the highest-frequency arc corresponds to bulk conductivity, which is obtained from the real-axis intercept, i.e., the highest resistance value of this arc.

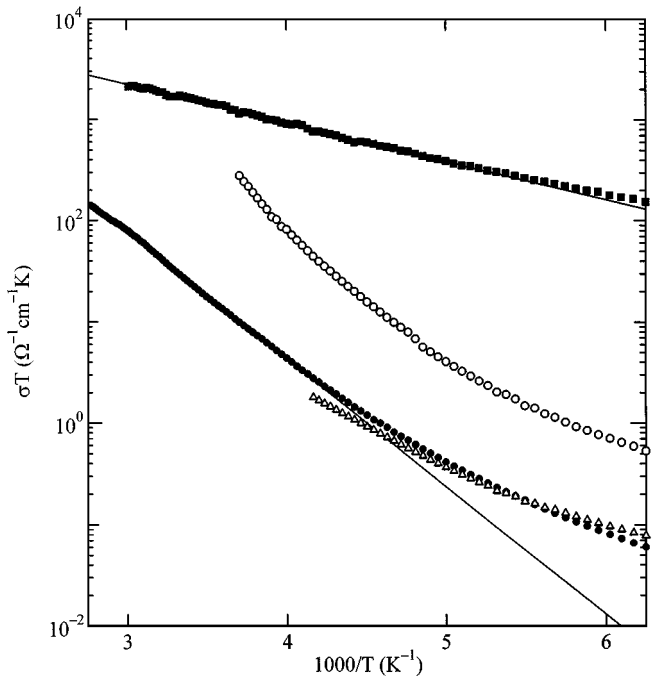

FIG. 3. Arrhenius relations of σT versus $1/T$. Solid circles and squares are four-probe dc conductivity for the specimens with $x = 0.1$ and 0.5. Open triangles and circles are conductivity estimated from the highest resistance values of the intermediate-frequency arcs and the bulk conductivity for the specimen with $x = 0.1$. The highest resistance value of the intermediate-frequency arc corresponds to concuction across grain boundaries. This resistance is obtained from the real-axis intercept of this arcs. Straight lines represent linear portions in Arrhenius plots of dc conductivity and $1/T$.

energy estimated in bulk conductivity, i.e., $W_H \cong 0.26$ eV. With increasing x from 0.1 to 0.5, however, hopping energy reduces rapidly to $W_H = 0.075$ eV for $x = 0.5$.

There is further evidence for adiabatic hopping process of small polarons in this system. If a dielectric relaxation process is of this mechanism, the characteristic frequency at the maximum of the Cole–Cole circular arc, f_{max}, is the lower limit of the dc hop frequencies which is related to R and C as follows (41):

$$2\pi f_{max} RC = 1, \qquad [2]$$

where $C = (\varepsilon_0 - \varepsilon_\infty)\varepsilon_0$ (ε_0, ε_∞, and ε_0 being the static dielectric constant, the optical dielectric constant, and the permittivity of free space, respectively), and R is the resistance. Figure 4 shows the Cole–Cole plots at 230, 250, and 270 K for the specimen with $x = 0.1$, where the solid lines are the circular arcs calculated by the least-mean-square analysis, using the experimental plots. Equation [2] means that the characteristic frequencies, f_{max}, estimated from the maxima of the circular arcs provide conductivities; i.e., $1/R = 2\pi f_{max} C$. The conductivities obtained in this way are $2.89 \times 10^{-3}\ \Omega^{-1}\,cm^{-1}$ at 230 K, $6.73 \times 10^{-3}\ \Omega^{-1}\,cm^{-1}$ at 250 K, and $2.05 \times 10^{-2}\ \Omega^{-1}\,cm^{-1}$ at 270 K, respectively. There are good agreements, although the conductivities estimated from Cole–Cole plots are slightly small in value compared with four-probe dc conductivities. This result is consistent with the conclusion of the conduction being due to the hopping process of small polarons in $x = 0.1$ as described before.

The legitimacy of adiabatic hopping conduction in the $La_{0.9}Sr_{0.1}Fe_{1-x}Co_xO_3$ system is evidenced by a dielectric relaxation process as well as our previous works (16, 24–33). Figure 5 displays frequency dependencies of dielectric loss factor ε'' for the specimen with $x = 0.1$ at 10 K increments in the range of 210 to 280 K over the frequency up to 1 MHz. In the specimen with $x = 0.5$, a dielectric relaxation process also occurs at $T < 150$ K. Since this low-temperature range is very close to spin-glass freezing temperature T_g which is estimated to be about 60 K as described later, it is practically impossible to obtain experimental knowledge on this relaxation process. According to Debye's theory, the resonance frequency of dielectric loss factor has a form,

$$f_{\varepsilon''} \propto \exp\left(-\frac{Q}{k_B T}\right), \qquad [3]$$

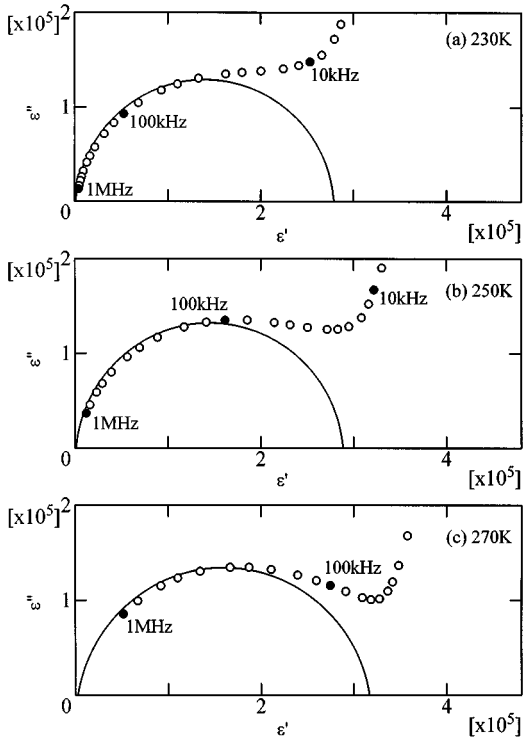

FIG. 4. Cole–Cole plots for $La_{0.9}Sr_{0.1}Fe_{1-x}Co_xO_3$ specimen with $x = 0.1$ at several temperatures, (a) 230 K, (b) 250 K, and (c) 270 K, where ε' and ε'' represent dielectric constant and dielectric loss at each applied frequency, respectively. The solid lines are the circular arcs calculated by the least-mean-square analysis.

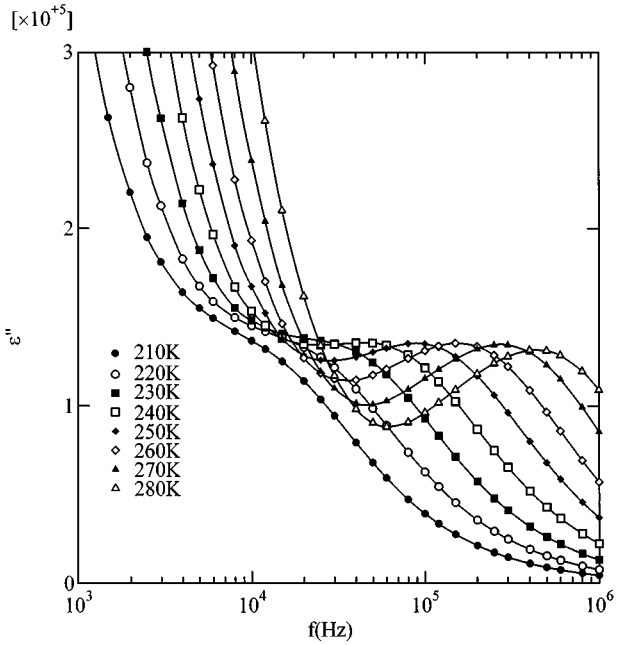

FIG. 5. Frequency dependencies of dielectric loss factor (ε'') as a parametric function of temperature of 210 to 280 K at 10 K increments for the specimen with $x = 0.1$.

where $f_{\varepsilon''}$ is the resonance frequency of ε'' at T, Q is the activation energy required for a dielectric relaxation, and $W_H \cong Q$ if a hopping process of small polarons is predominantly responsible for the dielectric relaxation (16, 24–33). Figure 6 plots the Arrhenius relation of $f_{\varepsilon''}$ and $1/T$ for the specimen with $x = 0.1$. The straight line at $T \geq 240$ K and the activation energy $Q = 0.26$ eV, which is nearly equal to W_H assure that a hopping process of small polarons dominates the electrical transport in the specimen with $x = 0.1$. The similar scenario is also expected for $x = 0.5$ because of the linear relation in Arrhenius plots at $T \geq 185$ K in Fig. 3.

Though the conduction kinetics does not change even if x increases from 0.1 to 0.5, hopping energy decreases rapidly as the amount of Co ions increases. As described in the Introduction, the majority of carriers in both end members, $La_{0.9}Sr_{0.1}FeO_3$ and $La_{0.9}Sr_{0.1}CoO_3$, are ligand holes due to strongly hybridized $3d$–$2p$ bands, and then the nature of carriers in $La_{0.9}Sr_{0.1}Fe_{1-x}Co_xO_3$ must not alter even if x increases from 0.1 to 0.5. The peculiar characteristic in the carrier then does not account for such a huge reduction in hopping energy. Since hopping energy has the theoretical form,

$$W_H = \frac{W_P}{2} - t, \qquad [4]$$

where W_P is polaron binding energy and t is bandwidth (40), such a huge reduction in W_H implies that an increase in Co content either reduces polaron binding energy or broadens bandwidth. This phenomenon must be strongly related to the crystallographic transfer from orthorhombic (*Pbnm*) to rhombohedral structure ($R\bar{3}C$) with increasing x. The space group symmetry heightens as x increases from 0.1 to 0.5. Since Fermi level in $La_{0.9}Sr_{0.1}Fe_{1-x}Co_xO_3$ may be composed of M $3d$ and O $2p$ orbital, bandwidth is governed by a M–O^{2-}–M bond angle which is represented by ($180°$–Θ) when it deviates from $180°$, where M stands for a transition-metal element. As the space group symmetry heightens, Θ decreases (42). This is evidenced by the neutron diffraction study on $La_{0.7}Sr_{0.3}Fe_{1-x}Co_xO_3$ which shows that replacement of Fe ion with Co ion decreases Θ (20). Since a large deviation of M–O^{2-}–M bond angle from $180°$ localizes deeply charge carriers resulting in a large magnitude for W_P, an increase in the amount of Co ions advances delocalization of charge carriers and then decreases W_P because the space group symmetry heightens from *Pbnm* to $R\bar{3}C$ with increasing x. Furthermore, M $3d$ and O $2p$ wave functions overlap more as M–O^{2-}–M bond angle increases toward $180°$, accordingly resulting in an enlargement in bandwidth. Then variations in both polaron binding energy and bandwidth with increasing x are mainly responsible for such a rapid reduction in hopping energy.

3.3. Magnetic Properties

Figure 7 demonstrates temperature dependencies of magnetic susceptibility χ measured in the magnetic field of 1 T after cooling the specimen down to 10 K in the magnetic field of 1 T (FC) or in the zero field (ZFC) for $x = 0.5$. Despite Fe-antiferromagnetism included in $(La,Sr)Fe_{1-x}Co_xO_3$ (20), the FC curve has a ferromagnetic feature, which must result from Co ions. Around 60 K, the ZFC curve involves a cusp that is assigned to the spin blocking behavior due to weak ferromagnetic interaction, as is usually observed in spin-glass systems (19). Then, T_g is approximately 60 K. A large deviation of the ZFC curve from FC below T_g indicates that short-range ferromagnetic orders

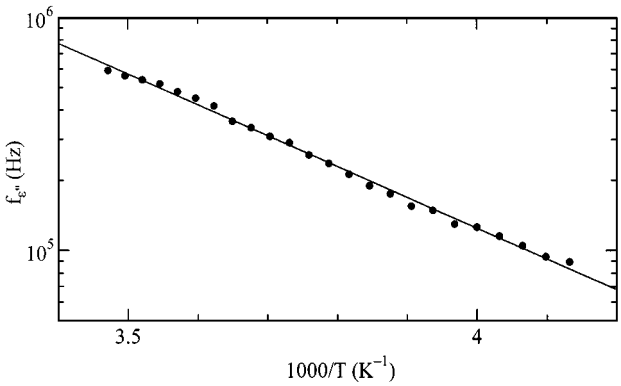

FIG. 6. Arrhenius relations between $f_{\varepsilon''}$ and $1/T$ for the specimen with $x = 0.1$.

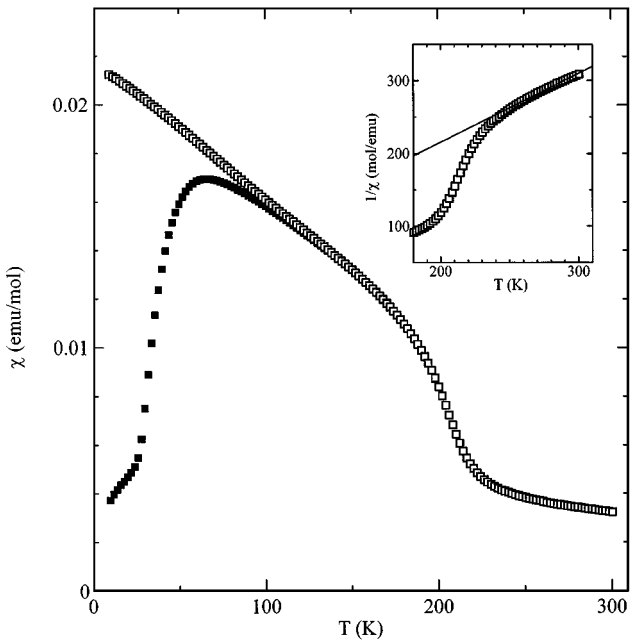

FIG. 7. Temperature dependence of χ in the field of 1 T under FC (open squares) and ZFC (solid squares) for the specimen with $x = 0.5$. The inset shows the relation of $1/\chi$ versus T above 180 K and the straight line represents a Curie–Weiss relation for the specimen with $x = 0.5$ at 240 K $< T <$ 300 K.

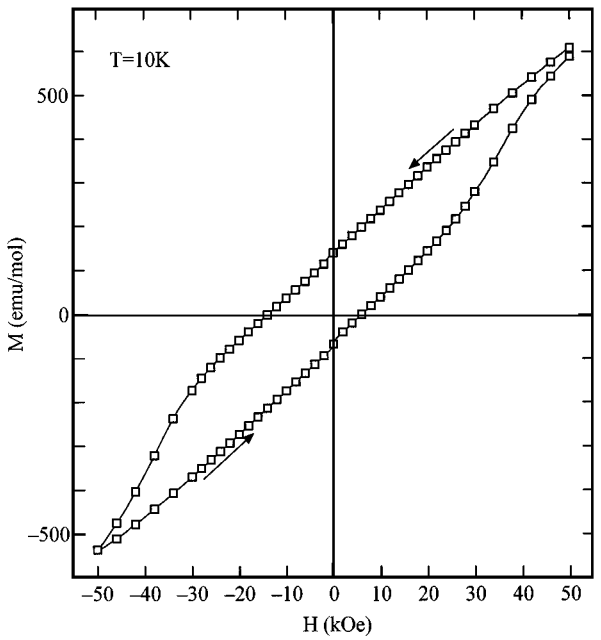

FIG. 8. ZFC magnetization M versus applied field H of $x = 0.5$ at 10 K.

work effectively instead of simple long-range ferromagnetic orders. In the specimen with $x = 0.5$, DE interaction between Co ions via O^{2-} must be mainly responsible for short-range ferromagnetic interaction. Two couplings are possible for DE interaction, i.e., IS Co^{3+} $(t_{2g}^5 e_g^1)$–O^{2-}–LS Co^{4+} (t_{2g}^5) or HS Co^{3+} $(t_{2g}^4 e_g^2)$–O^{2-}–IS Co^{4+} $(t_{2g}^4 e_g^1)$. Other couplings are inadequate because one of t_{2g} electrons in Co ion has to contribute to electronic transport as a charge carrier (21–23). As temperature rises from T_g, DE interaction decays, and one expects that all or most Co ions in this material are IS Co^{3+} and LS Co^{4+} if IS Co^{3+}–O^{2-}–LS Co^{4+} DE interaction is dominant below T_g, or that only HS Co^{3+} and IS Co^{4+} exist if HS Co^{3+}–O^{2-}–IS Co^{4+} DE interaction is mainly responsible for the spin-glass phase.

Figure 8 provides further evidence of spin-glass behavior for the specimen with $x = 0.5$ below T_g. At 10 K the magnetization M versus applied field H curve of the ZFC sample shows no saturation at 50 kOe; lack of saturation in high fields is a characteristic feature of spin glasses (43). Moreover, Itoh *et al.* (19) have shown an aging effect in the magnetization of ZFC samples, which is another characteristic feature of spin-grass phases.

Curie–Weiss relation holds at $T \geq 250$ K for the specimen with $x = 0.5$, as shown in the inset in Fig. 7, which plots χ^{-1} against T above 180 K. The experimental magnitude for Curie constant ($C = 1.06$ emu K/mol) yields $\mu_{eff} = 2.91\mu_B$, where $\mu_{eff} \cong \sqrt{8C}\mu_B$, μ_{eff} is the effective magnetic moment and μ_B is Bohr magneton. If localized spins on HS Co^{3+} and IS Co^{4+} mainly contribute to paramagnetism at $T \geq 250$ K in the specimen with $x = 0.5$, the effective magnetic moment estimated theoretically is $2.78\mu_B$, which is comparable with the experimental value, $2.91\mu_B$. If Co ions in the specimen with $x = 0.5$ are mostly IS Co^{3+} and LS Co^{4+}, the calculated effective magnetic moment is $1.67\mu_B$, which differs considerably from the experimental value. These estimations surmise that all or most of Co ions in $La_{0.9}Sr_{0.1}Fe_{0.5}Co_{0.5}O_3$ are HS Co^{3+} and IS Co^{4+}. These results indicates marked Co-effects on magnetic properties in $La_{0.9}Sr_{0.1}Fe_{1-x}Co_xO_3$.

3.4. Thermopower

The experiment on thermopower also provides important knowledge on Co states in $La_{0.9}Sr_{0.1}Fe_{1-x}Co_xO_3$. The theoretical formula of thermopower S for insulating materials has a form,

$$S = \pm \frac{k_B}{e}\left(\frac{E_S}{k_B T}\right) + S_\infty, \qquad [5]$$

where S_∞ is the $T \to \infty$ limit of thermopower (44). Figure 9 demonstrates temperature dependence of the thermopower for the specimens with $x = 0.1$ and 0.5 above 167 K. Because of high resistance, thermopower at low temperature was very difficult to measure in specimens with $x \leq 0.1$.

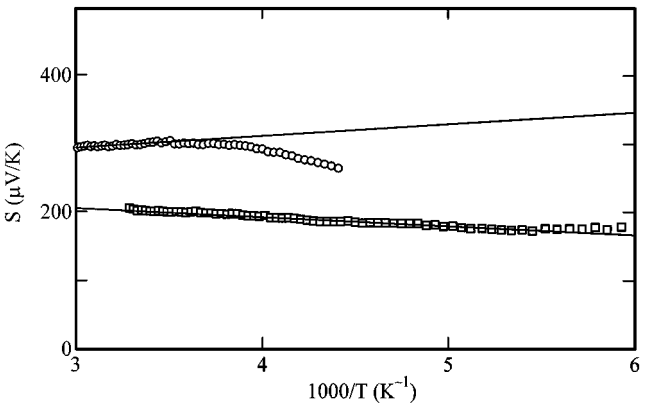

FIG. 9. Temperature dependence of thermopower (S) for the specimens with $x = 0.1$ (open circles) and $x = 0.5$ (open squares) above 167 K. The straight lines indicate the theoretical relation of Eq. [5].

Despite this, the theoretical relation of Eq. [4] holds at $T \geq 275$ K for $x = 0.1$. Thus, the temperature region in which the relation in Eq. [4] is observable experimentally for $x = 0.1$ is high and narrow in comparison with the region for $x = 0.5$. The least-mean-squares fitting methods yield $E_S = 0.018$ eV and $S_\infty = 241\ \mu$V/K for $x = 0.1$ and $E_S = 0.013$ eV and $S_\infty = 243\ \mu$V/K for $x = 0.5$. The large difference between W_H and E_S is a hallmark of polaronic transport (45, 46). In oxide where hopping motions of small polarons dominate electrical transports, E_S is the potential difference between identical lattice distortions with and without a hole and/or an electron (47), while W_H is the hopping energy of small polarons and generally $W_H \gg E_S$. Indeed, Holstein predicted that the thermally activated drift mobility of small polarons causes W_H to differ from E_S in an amount of one half of the formation energy of polarons (39, 48).

Recently, Koshibae *et al.* (34, 35) have carried out the theoretical work on thermopower, generalizing Heikes formula and extended the high-temperature limit theory to the strong correlation system such as $La_{1-c}Sr_cMO_3$. Thermopower in the high-temperature limit is then given by

$$S_\infty = -\frac{k_B}{e} \ln\left(\frac{g_3}{g_4}\frac{c}{1-c}\right), \qquad [6]$$

where c is the concentration of M^{4+} ions, c being then 0.1 in the present system, and g_3 (g_4) is the spin and orbital degree of freedom at the M^{3+} (M^{4+}) site. In the case of $La_{0.9}Sr_{0.1}FeO_3$ ($x = 0.0$), Fe ions in are in HS states (2, 3), and it is reasonably accepted that 90% of Fe ions is HS Fe^{3+} ($t_{2g}^3 e_g^2$) and the rest is HS Fe^{4+} ($t_{2g}^3 e_g^1$). Then M^{3+} and M^{4+} in this material are HS Fe^{3+} and HS Fe^{4+}. Following the theoretical treatment of Koshibae *et al.* (34, 35), $g_3 = 6$ and $g_4 = 10$, so that S_∞ has the value of 233 μV/K.

As described in the speculation on magnetic results for $x = 0.5$, two combinations of ionic species included in $La_{0.9}Sr_{0.1}Fe_{0.5}Co_{0.5}O_3$ are possible; namely, one is (i) HS Fe^{3+}, HS Fe^{4+}, IS Co^{3+}, and LS Co^{4+} and the other is (ii) HS Fe^{3+}, HS Fe^{4+}, HS Co^{3+}, and IS Co^{4+}. Assuming that the similar situation also holds in the specimen with $x = 0.1$, S_∞ is estimated theoretically in $La_{0.9}Sr_{0.1}(Fe_{0.9}^{3+}Fe_{0.1}^{4+})_{1-x}$ $(Co_{0.9}^{3+}Co_{0.1}^{4+})_xO_3$ ($x = 0.1$ and 0.5) by using Eq. [6], where $c = 0.1$. If all or most of ions in this compound are in the case of (i), g_3 is 24, which is obtained by the sum of the degeneracies of HS Fe^{3+} and IS Co^{3+} site, i.e., 6 + 18, and $g_4 = 10 + 6 = 16$, which is given by the degeneracies of HS Fe^{4+} and LS Co^{4+} site (34, 35). However, these magnitudes yield $S_\infty = 154\ \mu$V/K, which differs considerably from the experimental values. In the case of (ii), on the other hand, gs are given by $g_3 = 6 + 15 = 21$ and $g_4 = 10 + 24 = 34$ (34, 35). Consequently, $S_\infty = 231\ \mu$V/K, which is very close to the experimental values, i.e., 241 μV/K for $x = 0.1$ and 243 μV/K for $x = 0.5$. From these estimations, thermopower results deduce that all or most of Co ions in $La_{0.9}Sr_{0.1}Fe_{1-x}Co_xO_3$ are HS Co^{3+} and IS Co^{4+} ions, which are in good agreement with the surmise based upon the estimation of effective magnetic moment.

4. CONCLUSION

Variations in physical properties due to a change in Co content in $La_{0.9}Sr_{0.1}Fe_{1-x}Co_xO_3$ ($x \leq 0.5$) have been investigated so as to elucidate Co states because short range ferromagnetic orders are expected to dominate magnetic properties in this system at a rather large x, although Fe-antiferromagnetism must govern magnetic properties when x is very small. Arrhenius relation of σT and $1/T$ holds for both $x = 0.1$ and 0.5. This indicates that hopping conduction dominates electronic transport properties at $x \leq 0.5$. A dielectric relaxation observed in ac measurements for $x = 0.1$ supports this surmise. There is, however, a huge reduction of hopping energy from 0.26 to 0.075 eV with increasing x from 0.1 to 0.5. This reduction comes from a decrease in polaron binding energy and an enlargement in bandwidth through the crystallographic transfer from orthorhombic (*Pbnm*) to rhombohedral structure ($R\bar{3}C$) induced by an increase in Co content. A spin-glass phase due to short-range ferromagnetic orders is recognized for $x = 0.5$ in magnetic measurements because the ZFC curve for $x = 0.5$ involves a cusp that is assigned to the spin-glass behavior due to a weak ferromagnetic interaction. Curie–Weiss relation realized in the specimen of $x = 0.5$ yields $\mu_{eff} = 2.91\mu_B$, which deduces that all or most of Co ions included in this material are HS Co^{3+} and IS Co^{4+}. Thermopower in the high-temperature limit estimated theoretically under the assumption that $La_{0.9}Sr_{0.1}Fe_{1-x}Co_xO_3$ contains mostly HS Co^{3+} and IS Co^{4+} is close in value to

magnitudes estimated experimentally at $T \to \infty$. The most significant Co effect in $La_{0.9}Sr_{0.1}Fe_{1-x}Co_xO_3$ is to enhance HS Co^{3+}–O^{2-}–IS Co^{4+} double-exchange interaction which results in short range ferromagnetic orders when x is large.

ACKNOWLEDGMENTS

This work was supported by a Grant-in-Aid for Science Research (No. 11650716) from the Ministry of Education, Science, and Culture and by Takahashi Industrial and Economic Research Foundation. The dc conductivity and thermopower were measured at Instrumental Analysis Center in Yokohama National University. The SQUID magnetometer in Ecotechnology System Laboratory, Yokohama National University, was used.

REFERENCES

1. J. C. Grenier, N. Ea, M. Pcchard, and M. M. Abou-Sekkina, *Mater. Res. Bull.* **19,** 1301 (1984).
2. M. Abbate, F. M. F. de Groot, J. C. Fuggle, A. Fujimori, O. Strebel, F. Lopez, M. Domke, G. Kaindl, G. A. Sawatzky, M. Takano, Y. Takeda, E. Eisaki, and S. Uchida, *Phys. Rev. B* **46,** 4511 (1992).
3. A. Chainani, M. Mathew, and D. D. Sarma, *Phys. Rev. B* **48,** 14818 (1993).
4. P. M. Raccah and J. B. Goodenough, *Phys. Rev.* **155,** 932 (1967).
5. M. A. Señarís-Rodríguez and J. B. Goodenough, *J. Solid. State. Chem.* **116,** 224 (1995).
6. A. Chainani, M. Mathew, and D. D. Sarma, *Phys. Rev. B* **46,** 9976 (1992).
7. R. Mathendiran and A. K. Raychaudhuri, *Phys. Rev. B* **54,** 16044 (1996).
8. V. Golovanov, L. Mihaly, and A. R. Moodenbaugh, *Phys. Rev. B* **53,** 8207 (1996).
9. M. H. R. Lankhorst, H. J. M. Bouwmeester, and H. Verweij, *Phys. Rev. Lett.* **77,** 2989 (1996).
10. T. Saitoh, T. Mizokawa, A. Fujimori, M. Abbate, Y. Takeda, and M. Takano, *Phys. Rev. B* **56,** 1290 (1997).
11. H. Takahashi, F. Munakata, and M. Yamanaka, *Phys. Rev. B* **57,** 15211 (1998).
12. M. R. Ibarra, R. Mahendiran, C. Marquina, B. García-Landa, and J. Blasco, *Phys. Rev. B* **57,** R3217 (1998).
13. R. Caciuffo, D. Rinaldi, G. Barucca, J. Mira, J. Rivas, M. A. Señarís-Rodríguez, P. G. Radaelli, D. Fiorani, and J. B. Goodenough, *Phys. Rev. B* **59,** 1068 (1999).
14. M. A. Señarís-Rodríguez and J. B. Goodenough, *J. Solid State Chem.* **118,** 323 (1995).
15. R. H. Potze, G. A. Sawatzky, and M. Abbate, *Phys. Rev. B* **51,** 11501 (1995).
16. E. Iguchi, K. Ueda, and H. Nakatsugawa, *J. Phys.*: *Condens. Matter* **10,** 8999 (1998).
17. V. G. Bhide, D. S. Rajoria, C. N. R. Rao, and V. G. Jadhao, *Phys. Rev. B* **12,** 2832 (1975).
18. V. G. Sathe, A. V. Pimpale, V. Siriguri, and S. K. Paranjpe, *J. Phys.*: *Condens. Matter* **8,** 3889 (1996).
19. M. Itoh, I. Natori, S. Kubota, and K. Motoya, *J. Phys. Soc. Jpn.* **63,** 1486 (1994).
20. V. G. Sathe, S. K. Paranjpe, V. Siruguri, and A. V. Pimpale, *J. Phys. Condens. Matter* **10,** 4045 (1998).
21. C. Zener, *Phys. Rev.* **81,** 440 (1951).
22. C. Zener, *Phys. Rev.* **82,** 403 (1951).
23. P. G. De Gennes, *Phys. Rev.* **118,** 141 (1960).
24. E. Iguchi and W. H. Jung, *J. Phys. Soc. Jpn.* **63,** 3078 (1994).
25. W. H. Jung and E. Iguchi, *J. Phys. Condens. Matter* **7,** 1215 (1995).
26. W. H. Jung and E. Iguchi, *Philos. Mag. B* **73,** 873 (1996).
27. E. Iguchi, K. Ueda, and W. H. Jung, *Phys. Rev. B* **54,** 17431 (1996).
28. E. Iguchi, N. Nakamura, and A. Aoki, *J. Phys. Chem. Solids* **58,** 755 (1997).
29. W. H. Jung, H. Nakatsugawa, and E. Iguchi, *J. Solid State Chem.* **133,** 466 (1997).
30. E. Iguchi, N. Nakamura, and A. Aoki, *Philos. Mag. B* **78,** 65 (1998).
31. W. H. Jung and E. Iguchi, *J. Phys. D* **31,** 794 (1998).
32. E. Iguchi, H. Nakatsugawa, and K. Futakuchi, *J. Solid. State. Chem.* **139,** 176 (1998).
33. H. Nakatsugawa and E. Iguchi, *J. Phys. Condens. Matter* **11,** 1711 (1999).
34. W. Koshibae, K. Tsutui, and S. Maekawa, *Phys. Rev. B* **62,** 6869 (2000).
35. W. Koshibae, *pers. commun*.
36. J. E. Bauerle, *J. Phys. Chem. Solids.* **30,** 2657 (1969).
37. J. R. MacDonald, *J. Chem. Phys.* **61,** 3977 (1974).
38. A. D. Franklin, *J. Am. Ceram. Soc.* **58,** 465 (1975).
39. D. Emin and T. Holstein, *J. Am. Ceram. Soc.* **53,** 439 (1969).
40. I. G. Austin and N. F. Mott, *Adv. Phys.* **18,** 41 (1969).
41. L. L. Hench and J. K. West, "Principles of Electronic Ceramics," p. 205. Wiley, New York, 1990.
42. "Landolt–Börnstein New Series," Group III, Vol. 4a. Springer, Berlin, 1970.
43. J. A. Mydosh, *in* "Spin Glasses. An Experimental Introduction." Taylor & Francis, London, 1993.
44. P. M. Chaikin and G. Beni, *Phys. Rev. B* **13,** 647 (1976).
45. M. Jaime, H. Hardner, M. B. Salmon, M. Rubinstein, P. Dorsey, and D. Emin, *J. Appl. Phys.* **81,** 4958 (1997).
46. E. Iguchi and N. Nakamura, *J. Phys. Soc. Jpn.* **68,** 1780 (1999).
47. M. Jaime, M. B. Salamon, M. Rubinstein, R. E. Treece, J. S. Horwitz, and D. B. Chrisey, *Phys. Rev. B* **54,** 11914 (1996).
48. L. Friedman and T. Holstein, *Ann. Phys*. **21,** 494 (1963).